Mechanical Systems and Signal Processing xxx (xxxx) xxx

Contents lists available at ScienceDirect

Mechanical Systems and Signal Processing

journal homepage: www.elsevier.com/locate/ymssp

An inverse identification strategy for the mechanical parameters of a phenomenological hysteretic constitutive model

Salvatore Sessa [a,*], Nicoló Vaiana [a], Massimo Paradiso [a], Luciano Rosati [a]

[a] Department of Structures for Engineering and Architecture, University of Naples Federico II, Via Claudio, 21, 80124 Napoli, Italy

ARTICLE INFO

Article history:
Received 18 October 2019
Received in revised form 17 December 2019
Accepted 4 January 2020
Available online xxxx

Keywords:
Inverse identification
Hysteretic materials
Bouc Wen model

ABSTRACT

An inverse strategy is developed for identifying the parameters of the hysteretic phenomenological constitutive model presented in Vaiana et al. (2019) and belonging to a wider class of hysteretic models. The model, differently from the celebrated Bouc-Wen one, permits the definition of either stress-strain or load-displacement relationships by closed-form expressions that do not require any iterative algorithm for the complete characterization of its response. The identification strategy is based on two optimization procedures performed in sequence in which a mean-square residual between a target and a computed response is minimized. The computation of suitable first trials is shown to represent an essential step of the procedure and is performed by taking advantage of the fact that its parameters correspond to physical quantities characterizing the experimental hysteretic loop. The procedure has been tested by identifying the mechanical parameters of two theoretical and four experimental responses for which numerical results prove the robustness and effectiveness of the proposed identification strategy.

1. Introduction

Constitutive models describing hysteretic behaviors play a widespread and significant role in several engineering applications. In general, the response of materials exhibiting hysteresis depends on the past history of the external actions besides their current value while it may be (for *rate-dependent* materials) or may not be (for *rate-independent* materials) influenced by the first time derivative of the action [1].

Applications of hysteretic models concern a large variety of scientific fields, mainly magnetics [2] and mechanics [3]. Within the field of structural engineering, hysteresis is involved in several applications involving ductile [4,5] and fragile materials [6], seismic devices [7–10], dampers [11,12] as well as for simulating the response of complex mechanical systems [13,14].

An important aspect for several applications concerns the convenience of adopting hysteretic models defined by means of a single function (instead of multi-linear ones) characterized by continuity conditions of the response and of its first derivative. This aspect has been highlighted for the case of random vibration applications [15,16] as well as for dynamic identification [17,18] and dynamic analysis of nanocomposites [19].

For this reason, several constitutive models have been proposed over years, the most widespread one being that due to Bouc [20] and later extended by Wen [16,21]. Its popularity depends on its capability of reproducing complex hysteretic

* Corresponding author.
E-mail address: salvatore.sessa2@unina.it (S. Sessa).

https://doi.org/10.1016/j.ymssp.2020.106622
0888-3270/

shapes with a limited number of constitutive parameters. Being ruled by differential equations involving the response and its first- or higher-order time derivative, the Bouc-Wen model belongs to the class of differential constitutive models which also includes further formulations [22,23]. Subsequently, such a model has been extended by several authors in order to account for a variety phenomena such as asymmetric [24] and degrading [15] hysteresis.

Although the main benefit of these differential formulations consists in their capability of reproducing a vast variety of hysteretic shapes and behaviors, they usually require numerical algorithms to be solved since closed-form solutions are available only for very peculiar cases [25]. Moreover, the presence of one or more differential equations to be solved strongly influences the procedures for determining the value of the constitutive parameters consistent with experimental data [26,27]. As an example, identification strategies of the Bouc-Wen parameters often involve complex procedures based on Bayesian inference [28,29], stochastic algorithms [30–32], polynomial approaches [33,34], genetic strategies [35] and differential evolution [36]. As discussed in [31], the main drawbacks affecting these strategies consist in the fact that most of them require to fix the value of some parameters to alleviate performance problems and, above all, that the pivotal estimation of the first trial parameters, which should be performed accordingly with the physics of the problem, is not straightforward.

Hysteretic models alternative to differential formulations are based on algebraic [37,38] and trascendental equations [39,40] although most of them were developed to describe a specific physical phenomenon so that their generalization, if possible, frequently presents significant limitations.

Within the framework of rate-independent, non-degrading symmetric hysteresis, a new class of uniaxial constitutive models has been recently proposed [41–43]. Such models are capable of modeling a broad variety of hysteretic behaviors by means of smooth curves whose expression is determined analytically.

Compared to the models available in the literature, such a class provides curves quite similar to the Bouc-Wen model, at least in terms of hysteresis shape and of softening-hardening phenomena. Its implementation turns out to be very convenient since it does not require solution of any differential equation; hence, the models [41–43] are generally faster and computationally less demanding than the Bouc-Wen-like models. Moreover, their constitutive parameters represent physical properties that can be directly related to quantities deduced from experimental data.

Despite of the latter aspect, the identification of the constitutive parameters represents a key feature to the diffusion of the class of models [41–43]. In fact, an estimation based only on mechanical considerations or fitting experimental curves, although effective in determining the magnitude of the parameters, lacks a sufficient accuracy and does not provide a measure of the errors.

To overcome such an issue, this research presents a rational and systematic strategy for identifying the constitutive parameters of the hysteretic model [43]. This has been chosen since it is the most advanced and versatile of those belonging to the class proposed in [41].

The proposed strategy consists in two optimization procedures performed in sequence aiming to minimize a least-square residual between the numerical response and an experimental curve. Least-square optimization has been successfully employed in several identification problems with similar features and proved to be a robust easy-to-implement and effective strategy. Nevertheless, since optimization is carried out by means of iterative algorithms, it is essential to determine proper first trials of the identifying parameters in order to ensure convergence to the global minimum [44]. For this reason, the proposed strategy is focused on a phenomenological determination of the first trials which takes advantage of the physical interpretation of the identified constitutive model.

Compared to analogous strategies performed for the parameter identification of differential models, the proposed strategy does not require any limitation of the parameters' values nor assumes any approximation. On the contrary, the proposed strategy proved to be robust and does not require any particular expertise as it will be shown by the numerical applications.

The paper is organised as follows: Section 2 provides a summary of the class of hysteretic models presented in [41] while Section 2.1 summarizes the detailed formulation of the Algebraic Model presented in [42] which is currently the most advanced one of the class and has been implemented in OpenSees, an open source framework oriented for finite element analysis [45].

Such a model has been adopted by the identification procedure hereby proposed and formulated in Section 3 while Section 3.4 introduces some general rules which can be adopted for extending the presented procedure to any model belonging to the class.

Finally, numerical analyses to investigate the robustness of the proposed procedure and to show its effectiveness are reported in Section 4 while conclusions are discussed in Section 5.

2. A review of the hysteretic material class

The general formulation of the class of hysteretic materials presented in [41] and extended in [42] establishes a relationship between a generalized force f and a generalized displacement u. It consists in a combination of four types of curves, specifically, two (upper and lower) limiting curves, denoted as c_u and c_l, and two transition curves, c^+ and c^- relevant to positive and negative values of the velocity $\dot{u}$, respectively, see, e.g., Fig. 1(a).

The limiting curves c_u and c_l intercept the vertical axis at $\pm\bar{f}$. The generic transition curve c^+ has a starting point $[u_i^+, f(u_i^+)]$ on c_l and asymptotically tends to c_u; in particular, the distance between c^+ and c_u becomes smaller than a fixed tolerance δ at the displacement $u_j^+ = u_i^+ + 2u_0$. Analogously, the negative transition curve c^- begins on c_u and asymptotically tends to c_l.

Please cite this article as: S. Sessa, N. Vaiana, M. Paradiso et al., An inverse identification strategy for the mechanical parameters of a phenomenological hysteretic constitutive model, Mechanical Systems and Signal Processing, https://doi.org/10.1016/j.ymssp.2020.106622

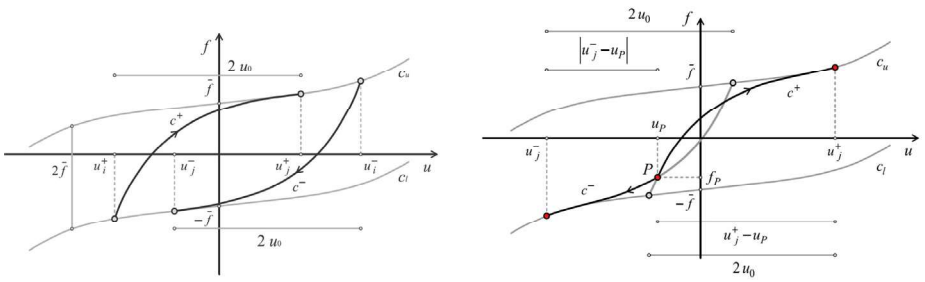

(a) Curves c_u, c_l, c^+ and c^- of a generic hysteresis loop

(b) Transition curves c^+ and c^- of a generic hysteresis loop

Fig. 1. Geometrical specifications of the hysteretic material class.

Each constitutive model belonging to the hysteretic class is defined by means of the generalized tangent stiffness expressed as function of the current displacement u and the relevant asymptotic displacement u_j^+ or u_j^-, depending on the algebraic sign of $\dot{u}$, as:

$$\begin{aligned} k_t\left(u, u_j^+\right) &= k_e(u) + k_h\left(u, u_j^+\right) \quad \text{for} \, \dot{u} > 0 \\ k_t\left(u, u_j^-\right) &= k_e(u) + k_h\left(u, u_j^-\right) \quad \text{for} \, \dot{u} < 0 \end{aligned} \tag{1}$$

in which functions k_e and k_h, though arbitrary, need to be integrable with respect to u.

The essential point of the hysteretic class consists in the fact that, given an arbitrary point (u_P, f_P), it is possible to univocally identify two transition curves c^+ and c^- so that they intersect at point P, as shown in Fig. 1(b). Consequently, the values of u_j^+ and u_j^- are also known. Thus, provided that k_t is integrable, the generalized force relevant to a displacement u turns out to be:

$$\begin{aligned} f(u) &= f_P + \int_{u_P}^{u} k_e(v)\, dv + \int_{u_P}^{u} k_h\left(v, u_j^+\right) dv \quad \text{for} \, \dot{u} > 0 \\ f(u) &= f_P + \int_{u_P}^{u} k_e(v)\, dv + \int_{u_P}^{u} k_h\left(v, u_j^-\right) dv \quad \text{for} \, \dot{u} < 0 \end{aligned} \tag{2}$$

We emphasize that the latter equations have been reported in an alternative form with respect to the original ones presented in [41] since they are more suitable for the description of the identification procedure.

Provided that the integrals of the functions k_e and k_h can be evaluated in closed form, the constitutive model can be exhaustively defined by an algebraic function and the generalized force can be computed in closed form avoiding numerical procedures.

Furthermore, to facilitate the implementation of the class of hysteretic models [41] in finite element frameworks, it is useful to introduce a symbolism consistent with the common practice in finite element analysis; thus, we shall denote by u_c and f, respectively, the generalized displacement and force at the last converged state, and by u_t is the trial value of the generalized displacement. Moreover, the algebraic sign of the generalized velocities are defined as:

$$\begin{aligned} s_c &= \text{sign}(\dot{u}_c) \\ s_t &= \text{sign}(\dot{u}_t) \end{aligned} \tag{3}$$

Furthermore, k_e and k_h depend upon a set of material parameters specific to each instance of the class formulated in [41]. Hence, in order to formulate the identification procedure regardless of the adopted constitutive model, it is useful to group the constitutive parameters into two vectors $\mathbf{x}_e$ and $\mathbf{x}_h$. Therefore, Eqs. (1) and (2) can be expressed as:

$$k_t(u_t, u_c, s_t, \mathbf{x}_e, \mathbf{x}_h) = k_e(u_t, \mathbf{x}_e) + k_h(u_t, u_c, s_t, \mathbf{x}_h) \tag{4}$$

$$f(u_t, u_c, s_t, \mathbf{x}_e, \mathbf{x}_h) = f_c + \int_{u_c}^{u_t} k_e(u, \mathbf{x}_e)\, du + \int_{u_c}^{u_t} k_h(u, u_c, s_t, \mathbf{x}_h)\, du \tag{5}$$

2.1. The algebraic hysteretic material

The Algebraic Model presented in [42] is based on a set of five parameters, namely $\mathbf{x}_h = [k_a, k_b, \alpha]$ defining k_h and $\mathbf{x}_e = [\beta_1, \beta_2]$ relevant to k_e. In particular, k_a is proportional to the initial stiffness of curves c^+ and c^-, k_b is the tangent stiffness of the limiting curves at $u = 0$ and α is a parameter which rules the passage between the transition and the limiting curves. Parameters β_1 and β_2 influence the shape of the limiting curves.

Please cite this article as: S. Sessa, N. Vaiana, M. Paradiso et al., An inverse identification strategy for the mechanical parameters of a phenomenological hysteretic constitutive model, Mechanical Systems and Signal Processing, https://doi.org/10.1016/j.ymssp.2020.106622

The model uses two auxiliary parameters defined as:

$$u_0 = \frac{1}{2}\left[\left(\frac{k_a - k_b}{\delta}\right)^{\frac{1}{2}} - 1\right]; \quad \bar{f} = \frac{k_a - k_b}{2}\left[\frac{(1+2u_0)^{1-\alpha} - 1}{1-\alpha}\right] \tag{6}$$

where δ denotes a geometric tolerance. Specifically, the response is computed by two transition curves c^+ and c^- which tend asymptotically to the limiting curves c_l and c_u. The discontinuity point between each transition curve and the corresponding limiting one corresponds to a gap which is not greater than δ.

The current value u_j of the asymptotic displacement is:

$$u_j = u_c + s_t(1+2u_0) - s_t\left(\frac{s_t(1-\alpha)}{k_a - k_b} f_c - \beta_1 u_c^3 - \beta_2 u_c^5 - k_b u_c - s_t\bar{f} + (k_a - k_b)\frac{(1+2u_0)^{1-\alpha}}{s_t(1-\alpha)}\right)^{\frac{1}{1-\alpha}} \tag{7}$$

and the trial force is given by:

$$f(u_t, u_c, s_t, \mathbf{x}_e, \mathbf{x}_h) = \beta_1 u_t^3 + \beta_2 u_t^5 + k_b u_t + (k_a - k_b)\left(\frac{(1 + s_t u_t - s_t u_j + 2u_0)^{1-\alpha}}{s_t(1-\alpha)} - \frac{(1+2u_0)^{1-\alpha} - 1}{1-\alpha}\right) + s_t\bar{f} \tag{8}$$

Note that the tangent stiffness turns out to be:

$$k_t(u_t, u_c, s_t, \mathbf{x}_e, \mathbf{x}_h) = \frac{df}{du_t} = 3\beta_1 u_t^2 + 5\beta_2 u_t^4 + k_b + s_t(k_a - k_b)(1 + s_t u_t - s_t u_j + 2u_0)^{-\alpha} \tag{9}$$

so that, recalling Eq. (4), k_e and k_h turn out to be:

$$\begin{aligned} k_e(u_t, \mathbf{x}_e) &= 3\beta_1 u_t^2 + 5\beta_2 u_t^4 \\ k_h(u_t, u_c, s_t, \mathbf{x}_h) &= k_b + s_t(k_a - k_b)(1 + s_t u_t - s_t u_j + 2u_0)^{-\alpha} \end{aligned} \tag{10}$$

3. Parameter identification procedure

To fix the ideas, let us consider an experimental response expressed by means of a load-displacement or stress-strain curve consisting in one or more hysteretic cycles as the one reported in Fig. 2(a).

Before starting the identification procedure, it is often necessary to delete the tips of the curve corresponding to the local maxima and minima of the displacement. In fact, curves to be identified are often determined by quasi-static experimental tests in which the response is affected by inertial contributions of the testing device. As a result, curves present smooth transitions of the response at those regions, corresponding to the tips of the hysteretic cycles, where the sign of the velocity is inverted.

Moreover, it is convenient to isolate each branch of the hysteretic cycles so that the identification can be performed separately for each one of them. Actually, the identification procedure presented in this section is based on a least-square minimization and is very sensitive to slight differences between the responses of different loops. Hence, even small differences between experimental cycles can affect the value of the identified parameters so that they could be not particularly representative of the physics of the experiment. In fact, the theoretical identified response will be a sort of average between the different cycles. Therefore, a global optimum, although capable of determining a good average of the response, can lack in reproducing appropriate stiffness trends, such as hardening and softening, since response derivatives are not taken into account by the procedure.

Considering that experimental data are usually provided in discrete form at fixed displacements $u_i, i = 1 \dots n$, where n is the number of the discretization steps, we collect the experimental values $f_e(u_i)$ relevant to a single branch of the hysteresis loop within the vector $\mathbf{f}_e$.

The identification procedure consists in a least-square optimization in which parameters are identified by minimizing the residual between the experimental response and the computed curve. Although least-squares optimization is not the sole

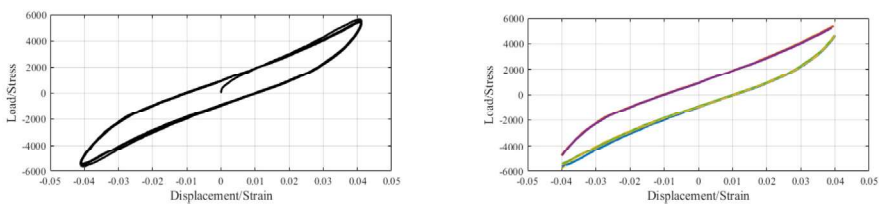

(a) Load-displacement response (displacements in m, forces in N)

(b) Branches of the experimental curve

Fig. 2. Sample of an experimental response relevant to a quasi-static uniaxial test of a wire rope isolator.

Please cite this article as: S. Sessa, N. Vaiana, M. Paradiso et al., An inverse identification strategy for the mechanical parameters of a phenomenological hysteretic constitutive model, Mechanical Systems and Signal Processing, https://doi.org/10.1016/j.ymssp.2020.106622

strategy useful for the parameter identification, it has been chosen mainly for its robustness in model parameter estimation [46]; moreover, it has been successfully used by the first Author to address even more complex problems [47,48].

To formulate the optimization problem, the residual $\boldsymbol{\Theta}(\mathbf{x}_e, \mathbf{x}_h)$ is defined as a vector whose i-th entry is defined by

$$\Theta(u_i, \mathbf{x}_e, \mathbf{x}_h) = \frac{f(u_i, u_{i-1}, s_t, \mathbf{x}_e, \mathbf{x}_h) - f_e(u_i)}{nf_e(u_i)} \tag{11}$$

so that the norm of $\boldsymbol{\Theta}(\mathbf{x}_e, \mathbf{x}_h)$ represents the squared-mean-square of the gap between the experimental data and the computational response associated with parameters $\mathbf{x}_e$ and $\mathbf{x}_h$.

The parameter identification is performed by solving the following optimization problem:

$$\begin{bmatrix} \hat{\mathbf{x}}_e \\ \hat{\mathbf{x}}_h \end{bmatrix} = \text{argmin}[\|\boldsymbol{\Theta}(\mathbf{x}_e, \mathbf{x}_h)\| | \mathbf{x}_e, \mathbf{x}_h] \tag{12}$$

where $\hat{\mathbf{x}}_e$ and $\hat{\mathbf{x}}_h$ are the identified values of $\mathbf{x}_e$ and $\mathbf{x}_h$ and the operator $\|\cdot\|$ denotes the norm of a vector and argmin$[f(\mathbf{x})|\mathbf{x}]$ denotes the argument $\mathbf{x}$ which minimizes the objective function $f(\mathbf{x})$.

In spite of its formal simplicity, the optimization problem of Eq. (12) must be carefully assessed. In fact, it is usually solved by adopting numerical algorithms such as the Interior Point algorithm [49] which has been adopted in this research.

For the case of strongly nonlinear residuals, the accuracy of the identified parameters depends on the starting point which is adopted for the minimization procedure since such algorithms can converge to local minima of the residual norm. For this reason, it is essential to estimate appropriate starting values for $\mathbf{x}_e$ and $\mathbf{x}_h$ in order to get confident about the identified parameters.

In general, an appropriate trial of $\mathbf{x}_h$ is far more easier to be estimated with respect to that of $\mathbf{x}_e$, at least for what concerns the order of magnitude. In fact, parameters of $\mathbf{x}_h$ are strongly related to physical quantities, such as forces and stiffness at given points, directly determined by the hysteretic branches.

3.1. Preliminary optimization

If we assume that the first trial of $\mathbf{x}_e$, denoted by $\mathbf{x}_e^0$, is set equal to zero (i.e., $\beta_1 = 0$ and $\beta_2 = 0$), the constitutive model defines an hysteretic branch consisting of straight lines connected by smooth curves, as reported in Fig. 3(a). In such a case, parameter k_a is the stiffness at the initial point of the loading curve while k_b is the stiffness of the upper and lower limiting lines. For this reason, it is possible to estimate the first trials k_a^0, k_b^0 and α^0 by conveniently analyzing the target curve.

In particular, the first trial of k_a can be directly evaluated by numerically computing the derivative of the experimental curve at its beginning point. Concerning k_b, it is useful to recall from [42] that the role of $k_e(u_t, \mathbf{x}_e)$ consists in determining deviations of the hysteretic curve from the straight lines determined by k_h. Moreover, Eq. (10) states that $k_e(0, \mathbf{x}_e) = 0$; thus, a good estimate of k_b can be computed as the slope of the line tangent to the experimental curve at the origin, as shown in Fig. 3(b).

A first trial α^0 of the parameter α can be computed, assuming u_0 to be unknown, by inverting Eq. (6). In this respect, we remind that u_0 represents half of the displacement for which the distance between the transition and the limiting curve becomes smaller than the tolerance δ, as shown in Fig. 1(a). Hence, a good estimate for u_0 can be obtained by setting $2u_0 = \Delta$ in which Δ is the amplitude of the experimental branch, as shown in Fig. 3(b).

Note that the latter assumption is not necessarily accurate; it is conventional and in general overestimates the real value of α. Nevertheless, its purpose is simply to estimate the magnitude of such a parameter in order to perform an optimization problem.

Finally, adopting the first trials k_a^0 and k_b^0 as stiffnesses and inverting Eq. 6_1, the first trial of α is:

$$\alpha^0 = \frac{\log\left[\left(k_a^0 - k_b^0\right)/\delta\right]}{\log\left(1 + \Delta\right)} \tag{13}$$

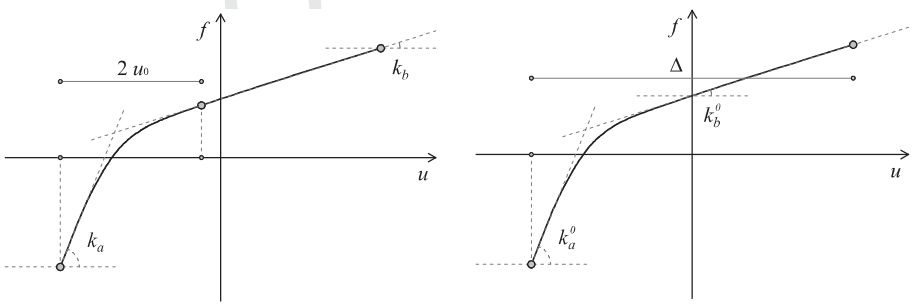

(a) Physical interpretation of k_a, k_b and u_0 (b) First trial values of k_a, k_b and Δ

Fig. 3. Estimation of the first trial values of the parameters determining $k_h(u)$.

Please cite this article as: S. Sessa, N. Vaiana, M. Paradiso et al., An inverse identification strategy for the mechanical parameters of a phenomenological hysteretic constitutive model, Mechanical Systems and Signal Processing, https://doi.org/10.1016/j.ymssp.2020.106622

The optimization procedure is then performed by an iterative algorithm and provides a first set of estimates $\hat{\mathbf{x}}_e^1 = \left(\hat{\beta}_1^1, \hat{\beta}_2^1\right)$ and $\hat{\mathbf{x}}_h^1 = \left(\hat{k}_a^1, \hat{k}_b^1, \hat{\alpha}^1\right)$ of the whole set of parameters:

$$\begin{bmatrix} \hat{\mathbf{x}}_e^1 \\ \hat{\mathbf{x}}_h^1 \end{bmatrix} = \text{argmin}[\|\boldsymbol{\Theta}(\mathbf{x}_e, \mathbf{x}_h)\| | \mathbf{x}_e, \mathbf{x}_h] \tag{14}$$

3.2. Refined optimization

In general, the preliminary optimization fails to determine the constitutive parameters with sufficient accuracy. In particular, the first trial of the optimization algorithm is esteemed as function of the stiffness at the loop edges and of the loop amplitude.

Estimation of the first trials of k_a, k_b and α performed in SubSection 3.1 is easy and straightforward as long as $\beta_1 = \beta_2 = 0$; conversely, evaluating a whole set of first estimates of the parameters is complex and unreliable.

The actual values for the parameters β_1 and β_2 can be significantly differ from zero, i.e. the initial trial values assumed for them. This can compromise the convergence of the algorithm to the global minimum.

For this reason, it is necessary to perform a further optimization after the estimation of more accurate first trials denoted as $\bar{\mathbf{x}}_e^0 = (\bar{\beta}_1^0, \bar{\beta}_2^0)$. In particular, the two scalar parameters $\bar{\beta}_1^0$ and $\bar{\beta}_2^0$ can be estimated by solving a system of two scalar equations. These can be obtained by imposing that the theoretical stiffness at given points is equal to the experimental stiffness of the hysteresis loop. Namely, denoting by u_k the displacement relevant to an arbitrary point belonging to the hysteresis loop, it is possible to determine the experimental value $k_{exp}(u_k)$ of the stiffness by finite differences. Then, we impose that the theoretical stiffness is equal to the experimental value:

$$k_e\left(u_k, \bar{\mathbf{x}}_e^0\right) + k_h\left(u_k, u_c, s_t, \hat{\mathbf{x}}_h^1\right) = k_{exp}(u_k) \tag{15}$$

in which stiffness k_h is computed by assuming the parameters $\hat{\mathbf{x}}_h^1 = \left(\hat{k}_a^1, \hat{k}_b^1, \hat{\alpha}^1\right)$ computed by the preliminary optimization and $\bar{\mathbf{x}}_e^0$ is the unknown variable.

Since $\bar{\mathbf{x}}_e^0$ has two components, it is necessary to choose two points u_1 and u_2 at which the values $k_{exp}(u_1)$ and $k_{exp}(u_2)$ are computed. In this respect, it is important that u_1 and u_2 are relevant to points of the hysteresis loop for which the sensitivity of k_e with respect to β_1 and β_2 is significant.

To this end we remark that the sensitivity of k_e with respect to the points with zero displacement is negligible, in fact, recalling Eq. (10),

$$k_e(0, \mathbf{x}_e) = 0 \quad \forall \mathbf{x}_e \tag{16}$$

Furthermore, as shown in [42], the role of the parameters $\mathbf{x}_e$ essentially consists in: i) introducing local maxima and ii) introducing hardening at the tip of the loop.

For this reason, the first significant point, whose displacement is denoted as u_1, is assumed to be located at the end of the loop. Moreover, if the experimental curve presents a local maximum at u_2, as shown in Fig. 4(a), it is convenient to adopt it as the second significant point since it represents a strong physical property of the hysteresis loop that can be conveniently used as constraint.

Should the curve be monotonic, u_2 can be set as a half of the maximum displacement of the loop, as shown in Fig. 4(b). This because it is not close to the origin, so that sensitivity of k_e should be not negligible, and is far enough from the loop edge, so that both significant points do not influence each other.

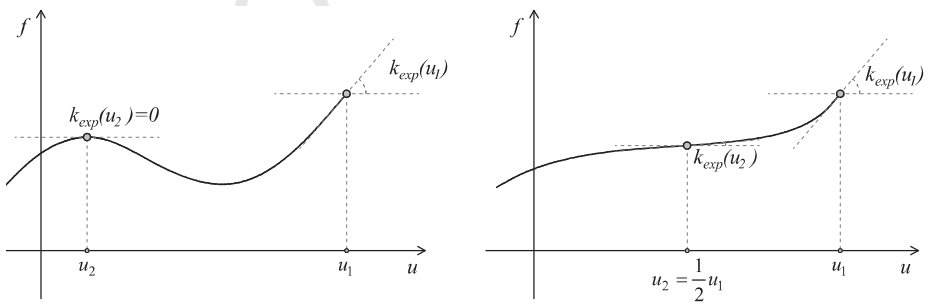

(a) Hysteresis with local maximum/minimum (b) Hysteresis with no local maximum/minimum

Fig. 4. *Significant points* adopted for the estimation of the first trials of the parameters β_1 and β_2.

Please cite this article as: S. Sessa, N. Vaiana, M. Paradiso et al., An inverse identification strategy for the mechanical parameters of a phenomenological hysteretic constitutive model, Mechanical Systems and Signal Processing, https://doi.org/10.1016/j.ymssp.2020.106622

Finally, the relevant stiffness values $k_{exp}(u_1)$ and $k_{exp}(u_2)$ are determined by applying finite differences to the experimental curve.

It is worth being emphasized that computation of $\bar{\mathbf{x}}_e^0 = (\bar{\beta}_1^0, \bar{\beta}_2^0)$ aims to determine a first trial to be used into an iterative algorithm; thus, it is possible to introduce some approximations while computing $\bar{\mathbf{x}}_e^0$. In this sense, we can assume that both significant points u_1 and u_2 are located on the limit curve. Therefore, recalling Eq. (9), the stiffness turns out to be:

$$k_t(u_t, u_c, s_t, \mathbf{x}_e, \mathbf{x}_h) = 3\beta_1 u_t^2 + 5\beta_2 u_t^4 + k_b \tag{17}$$

since:

$$\lim_{u_t \to \infty} k_b + s_t(k_a - k_b)\left(1 + s_t u_t - s_t u_j + 2u_0\right)^{-\alpha} = k_b \tag{18}$$

as shown in [43].

We can also assume that $k_b = \hat{k}_b^1$, i.e. the value obtained by the preliminary optimization. Thus, it is possible to determine the first trials of β_1 and β_2 by solving the linear system:

$$\begin{bmatrix} \bar{\beta}_1^0 \\ \bar{\beta}_2^0 \end{bmatrix} = \begin{bmatrix} 3u_1^2 & 5u_1^4 \\ 3u_2^2 & 5u_2^4 \end{bmatrix}^{-1} \begin{bmatrix} k_{exp}(u_1) - \hat{k}_b^1 \\ k_{exp}(u_2) - \hat{k}_b^1 \end{bmatrix} \tag{19}$$

and perform a further optimization analysis by an iterative algorithm defined as:

$$\begin{bmatrix} \mathbf{x}_e^\star \\ \mathbf{x}_h^\star \end{bmatrix} = \text{argmin}[\|\boldsymbol{\Theta}(\mathbf{x}_e, \mathbf{x}_h)\| | \mathbf{x}_e, \mathbf{x}_h] \tag{20}$$

having $\hat{\mathbf{x}}_h^1 = [\hat{k}_a^1, \hat{k}_b^1, \hat{\alpha}^1]^T$ and $\bar{\mathbf{x}}_e^0 = [\bar{\beta}_1^0, \bar{\beta}_2^0]^T$ as initial values. The identified constitutive parameters are denoted by $\mathbf{x}_e^\star$ and $\mathbf{x}_h^\star$.

For the reader's convenience, a summary of the proposed strategy is reported in the frame below.

3.3. Summary of the identification strategy

1. Fix a number of pairs $u_i, f_e(u_i)$ on the (discretized) experimental response of a single branch of the hysteretic loop; cut the tails if necessary;
2. Compute the first estimate $\mathbf{x}_h^0$ of parameters $\mathbf{x}_h$:
   - k_a^0 is the tangent stiffness at the beginning of the experimental branch;
   - k_b^0 is the tangent stiffness at the zero-displacement point of the experimental branch;
   - α^0 is computed by Eq. (13):

   $$\alpha^0 = \frac{\log\left[\left(k_a^0 - k_b^0\right)/\delta\right]}{\log(1+\Delta)}$$

3. Perform the *Preliminary Optimization* problem of Eq. (14)

   $$\begin{bmatrix} \hat{\mathbf{x}}_e^1 \\ \hat{\mathbf{x}}_h^1 \end{bmatrix} = \text{argmin}[\|\boldsymbol{\Theta}(\mathbf{x}_e, \mathbf{x}_h)\| | \mathbf{x}_e, \mathbf{x}_h]$$

   in order to get $\hat{\mathbf{x}}_e^1 = \left(\hat{\beta}_1^1, \hat{\beta}_2^1\right)$ and $\hat{\mathbf{x}}_h^1 = \left(\hat{k}_a^1, \hat{k}_b^1, \hat{\alpha}^1\right)$;
4. Determine the two significant points, represented either in Fig. 4(a) or 4(b), depending on the shape of the experimental curve, with displacements u_1 and u_2 and stiffness $k_{exp}(u_1)$ and $k_{exp}(u_2)$;
5. Solve the linear system of Eqs. (19):

   $$\begin{bmatrix} \bar{\beta}_1^0 \\ \bar{\beta}_2^0 \end{bmatrix} = \begin{bmatrix} 3u_1^2 & 5u_1^4 \\ 3u_2^2 & 5u_2^4 \end{bmatrix}^{-1} \begin{bmatrix} k_{exp}(u_1) - \hat{k}_b^1 \\ k_{exp}(u_2) - \hat{k}_b^1 \end{bmatrix}$$

   in order to get $\bar{\mathbf{x}}_e^0 = (\bar{\beta}_1^0, \bar{\beta}_2^0)$;
6. Perform the *Refined Optimization* problem of Eq. (20)

   $$\begin{bmatrix} \mathbf{x}_e^\star \\ \mathbf{x}_h^\star \end{bmatrix} = \text{argmin}[\|\boldsymbol{\Theta}(\mathbf{x}_e, \mathbf{x}_h)\| | \mathbf{x}_e, \mathbf{x}_h]$$

   starting from the trials $\hat{\mathbf{x}}_h^1 = \left(\hat{k}_a^1, \hat{k}_b^1, \hat{\alpha}^1\right)$ and $\bar{\mathbf{x}}_e^0 = (\bar{\beta}_1^0, \bar{\beta}_2^0)$ in order to get the identified parameters $\mathbf{x}_e^\star$ and $\mathbf{x}_h^\star$;

Please cite this article as: S. Sessa, N. Vaiana, M. Paradiso et al., An inverse identification strategy for the mechanical parameters of a phenomenological hysteretic constitutive model, Mechanical Systems and Signal Processing, https://doi.org/10.1016/j.ymssp.2020.106622

As a final remark, experimental hysteresis loops usually consist of more than a single cycle so that the identification procedure identifies the constitutive parameters relevant to each single branch separately. Thus, the average of the values computed by analyzing each branch is assumed as the comprehensive set of parameters that were looked for.

The presented strategy has proved to be stable and capable of addressing experimental loops with different shapes. Numerical applications to illustrate its capabilities are reported in Section 4.

The identification procedure has been specialized to the Algebraic Model [42] since it represents the most advanced model belonging to the phenomenological class [41] but it can be easily generalized, as discussed in the next subsection, by defining general rules to define firt trials of the two optimization procedures described above.

3.4. A possible generalization of the identification strategy

A common property of the mechanical models belonging to the phenomenological class presented in [41] consists in the fact that loops associated with stiffness k_h present linear behavior for both the limiting curves and the initial part of the transition curves. Such models differ by the specific formulation of the function ruling the transition phase between such linear parts.

For this reason, the identification strategy can still be performed by adopting the stiffness at the initial point of the hysteresis branch and at a suitable point of the limiting curve.

Depending on the shape of the experimental loop, these can be computed at specific points or, whenever the experimental data are not smooth, by trend lines evaluated over limited intervals.

Further parameters influencing the transition phase can be computed by determining the displacement intervals Δ_0 for which the limiting curve is reached, as represented in Fig. 5(a), as well as the force increment f_i associated with the displacement Δ_1 being the overall loop amplitude.

In general, it is necessary to adopt a number of experimental data equal to the number of required parameters. It is also important that, depending on the mathematical formulation of the constitutive model, these data are linearly independent.

Concerning the determination of the first trials to be adopted for the second optimization procedure, see, e.g., Steps 4 and 5 of the algorithm, it is possible to choose a set of significant points on the experimental hysteresis. Convenient points are represented by the extremal tip of the curve and points in which the curve presents local maxima and/or minima.

Fig. 5(b) shows a generic hysteretic branch in which some of the point of interest and their stiffnesses have been highlighted.

Each point represents an algebraic condition expressed by:

$$k_e(u_i, \mathbf{x}_e) + k_h\left(u_i, u_c, s_t, \hat{\mathbf{x}}_h^1\right) - k_{exp}(u_i) = 0 \tag{21}$$

and representing the i-th equation of a system in the unknown vector $\mathbf{x}_e$whose solution yields the trial estimate $\bar{\mathbf{x}}_e^0$. It is worth being emphasized that, if the specific constitutive model is conveniently formulated, the system of Eqs. (21) can be solved in closed form.

4. Numerical applications

In order to test the identification procedure proposed in Section 3 in conjunction with the Algebraic Model described in Section 2.1, a set of theoretical and experimental responses has been used as target of the identification algorithm.

The first four identifications have been carried out on the theoretical responses provided by the Algebraic Model associated with the sets of parameters reported in Table 1. Such procedures aim to investigate the consistency of the proposed

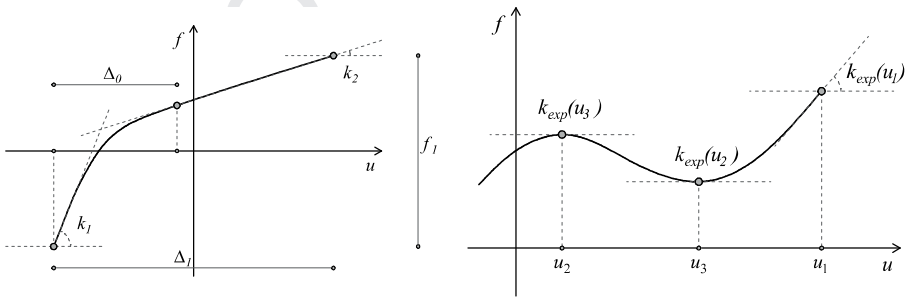

(a) Example of first trial values of the base curve (b) Example of *Significant Points* of a generic hysteretic branch

Fig. 5. Estimation of the first trial values of the parameters determining $k_h(u)$.

Please cite this article as: S. Sessa, N. Vaiana, M. Paradiso et al., An inverse identification strategy for the mechanical parameters of a phenomenological hysteretic constitutive model, Mechanical Systems and Signal Processing, https://doi.org/10.1016/j.ymssp.2020.106622

Table 1
Constitutive parameters of the Algebraic Model adopted for the identification of the theoretical response.

Test	k_a	k_b	α	β_1	β_2
AM1	100	10	20	−4	−1.5
AM2	120	5	30	−15	15
AM3	100	10	20	0	0
AM4	120	5	30	2	2

algorithm with the mechanical formulation of the constitutive model. In particular, the algorithm is expected to provide exactly the initial parameters adopted for the generation of the theoretical responses as well as null residuals.

Figs. 6(d) show the theoretical hysteresis loops of the Algebraic Model computed by assuming the values of Table 1. The reported curves represent the load-displacement target curve (represented in blue), the responses corresponding to the identified parameters, respectively, by the first and the second optimization procedure relevant to Steps 3 (green curve) and 6 (red curve) of the strategy summarized in Section 3.

As a matter of fact, the procedure exactly identifies the values of the assumed parameters and the residual turns out to be zero for both models.

In particular, the preliminary optimization procedure, representing Step 3 of the algorithm in Section 3.3, is sufficiently accurate to determine the parameters with no approximations. However, this phenomenon, which is not common in presence of experimental data, is due to the fact that the target curve is an artificial response computed by the very same constitutive model adopted for the identification procedure.

To investigate the capabilities of the proposed strategy in case of real applications, four experimental hysteresis loops have been adopted as target responses. The first one, shown in Fig. 8(a), is the mechanical response of a bolted Steel Reinforced Elastomeric Bearing (SREB) subject to dynamic actions tested by Tsai et al. [50]. It is a high-displacements rubber bearing having square cross section with dimensions 106 × 106 mm, 65 mm height and with thickness of the rubber layers of 41 mm.

A further experimental loop, shown in Fig. 8(b), is relevant to a Fiber Reinforced Rubber Bearer (FREB) tested by Kelly and Takhirov [51]; the bearer has circular cross section with diameter of 305 mm, height of 140 mm and thickness of rubber layers of 102 mm.

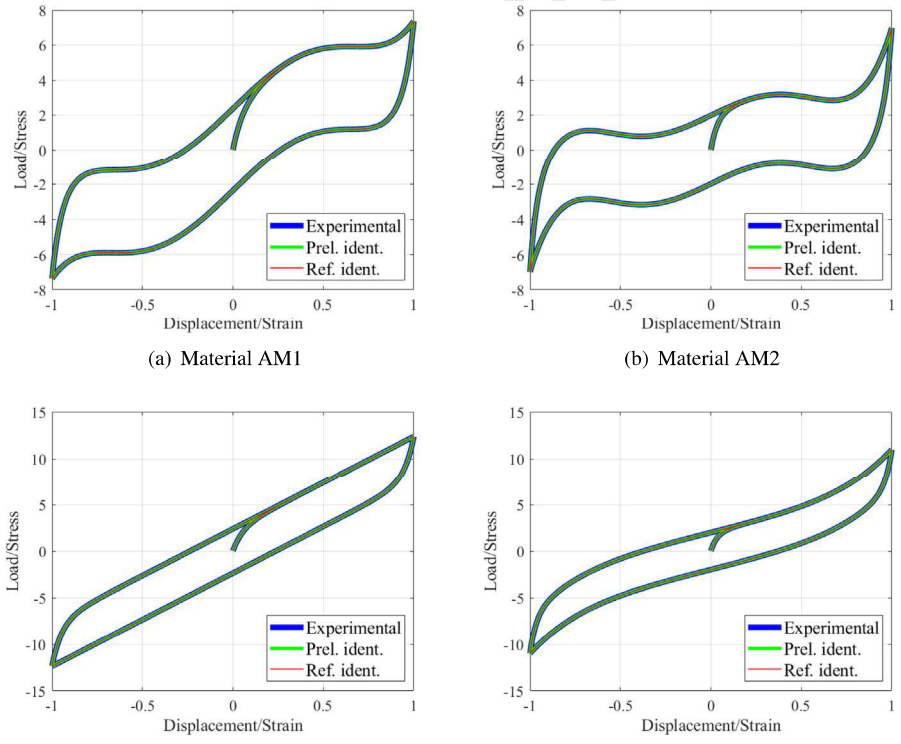

(a) Material AM1 (b) Material AM2

(c) Material AM3 (d) Material AM4

Fig. 6. Theoretical responses of the Algebraic Models with parameters of Table 1 and identified curves.

Please cite this article as: S. Sessa, N. Vaiana, M. Paradiso et al., An inverse identification strategy for the mechanical parameters of a phenomenological hysteretic constitutive model, Mechanical Systems and Signal Processing, https://doi.org/10.1016/j.ymssp.2020.106622

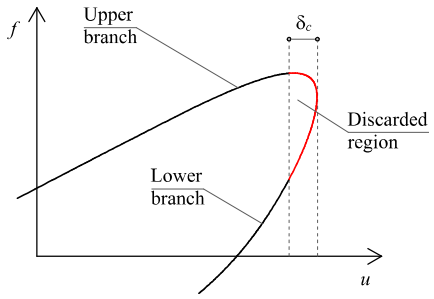

Fig. 7. Sample of a typical splitting of two consecutive branches of an hysteretic loop with deletion of the final tip region: δ_c depends on the particular hysteresis loop and ranges between 10^{-3} and $2 \cdot 10^{-4}$ in the assumed experiments.

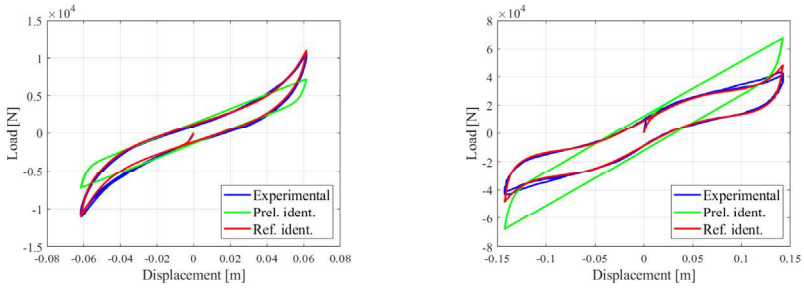

(a) SREB test (b) FREB test

Fig. 8. Target responses of the SREB and FREB experimental tests (blue curves) and identified curves with parameters of Tables 2 and 3.

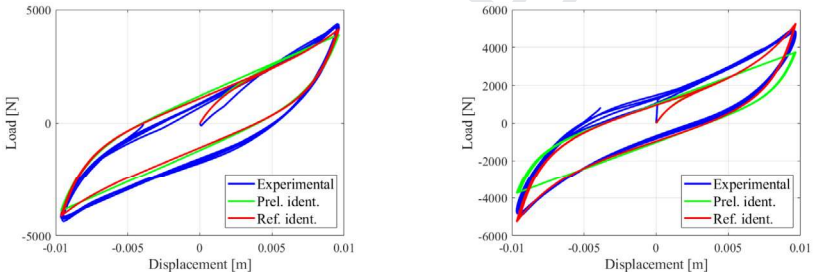

(a) PW16010L test (b) PW16010T test

Fig. 9. Target responses of the experimental tests (blue curves) and identified curves with parameters of Tables 2 and 3.

Two further loops, included in Fig. 9, correspond to the longitudinal and transverse experimental response of a wire-rope isolator type PWHS 16010 tested by Vaiana et al. [52]. The device has 267 mm length, 100 mm height, 110 mm width and 16 mm rope diameter. The device has been tested by applying loads along its longitudinal direction (test PW16010L) and along its transverse direction (test PW16010T).

The previous experimental responses have been selected to provide a comprehensive set of curves exhibiting different features that make more significant the numerical testing of the proposed procedure.

All experimental tests consisted in imposing a sinusoidal displacement, with specific amplitude and frequency, under the effect of an axial load; the recorded response is the horizontal reaction component along the displacement direction. We refer to the original papers for further details about the experimental protocols, which are omitted for brevity, since their load-displacement response is sufficient to perform the parameter identification. Tables reporting the values of the load-displacement response of such experimental tests can be downloaded at [53].

Each experimental response has been adopted as the target of the proposed identification strategy. In particular, hysteresis loops have been split into monotonic branches whose initial and final tips have been discarded in order to avoid inertial

Please cite this article as: S. Sessa, N. Vaiana, M. Paradiso et al., An inverse identification strategy for the mechanical parameters of a phenomenological hysteretic constitutive model, Mechanical Systems and Signal Processing, https://doi.org/10.1016/j.ymssp.2020.106622

effects of the testing machines. Fig. 7 reports a detail of a typical hysteresis loop in which the region affected by inertial phenomena is shown in red. The upper and lower branches are split and analyzed separately while the red region is deleted. The amplitude of the tip cuts, depending on each specific response, have been set equal to 0.0001 m for the SREB test, 0.001 m for the FREB test and 0.0002 for the PW16010L and PW16010T tests.

First trials of the preliminary optimization have been computed according to Step 2 of the strategy summarized in Section 3.1. For the reader's convenience, such values have been reported in columns 2-4 of Tables B.4–B.7 of Appendix B.

The residual has been defined according to Eq. (11) and the preliminary optimization of Step 3 of the algorithm has been performed by the Interior-Point algorithm [49,54,55], implemented in Matlab v. R2019a, with tolerance 10^{-8} and adopting the following bounds for the constitutive parameters within the optimization algorithm: $k_a > 0, k_b \leqslant k_a, \alpha \neq 1$.

The results of such first optimization are reported in Tables B.8–B.11 of Appendix B.

Such identified values have been used to determine the first trials of the refined optimization according to Steps 4 and 5 of the algorithm summarized in Section 3.3. The computed values are reported in columns 5-9 of Tables B.4–B.7 of Appendix B.

The refined optimization (Step 6) has been performed by adopting the residual of Eq. (11) and by using a Interior Point algorithm [49] implemented in Matlab with tolerance 10^{-12}. Bounds analogous to the ones adopted by the preliminary optimization were enforced by nonlinear transformations of the parameters.

Results of the refined optimization are reported in Tables B.12–B.15 of Appendix B.

Such a procedure has been repeated for each branch of the considered hysteresis loops. Obviously, for each one of them, a peculiar set of parameters has been identified. Thus, the identified values of the constitutive parameters relevant to each experimental test have been computed as averages of the values corresponding to each hysteresis branch.

The values of the constitutive parameters identified by the preliminary optimization of Step 3 of the algorithm are reported in Table 2 while Table 3 reports the parameters identified by the refined optimization corresponding to Step 6.

Figs. 8 and 9 report the load-displacement curves relevant to each identified test. In particular, the blue curves correspond to the experimental response; the green ones correspond to the response of the Algebraic Model defined by the parameters identified by the preliminary optimization (Table 2) while the red curves represent the response of the Algebraic Model computed by adopting the parameters identified by the refined optimization (Table 3).

The responses relevant to the parameters identified by the refined optimization show a very good matching with respect to the experimental ones, as confirmed by the values of the residuals at convergence, reported in the last column of Table 3. It is worth being emphasized that, although the identified curves tend to follow the experimental response, they catch significant features of the target loops such as hardening at the branch edges, stiffness trend and inflection points.

On the contrary, curves corresponding to the parameters identified by the preliminary optimization present very significant discrepancies with respect tot he experimental ones, as confirmed by the values of the residual at convergence reported in the last column of Table 2. As a matter of fact, the values of β_1 and β_2 identified by the preliminary identification (Table 2) present a magnitude which is significantly smaller than the one of the corresponding values identified by the refined optimization (Table 3). This difference is due to the fact that the preliminary identification assumes zero initial trials for β_1 and β_2 and such value is significantly far from the solution. For this reason, the sensitivity of the residual with respect to such parameters is negligible and the optimization converges to a local minimum.

This aspect confirms the needing to perform two separate optimization procedures (i.e., Steps 3 and 6) in order to correctly identify the constitutive parameters.

It is worth being emphasized that, for specific values of the parameter α, Eq. (6) provides complex values for u_0 and $\bar{f}$ as well as for the material response. Nevertheless, such an issue is generally avoided by the optimization procedure since a non-

Table 2
Averages of the identified constitutive parameters relevant to the experimental hysteresis loops. Preliminary optimization.

Test	k_a [N/m]	k_b [N/m]	α	β_1 [N/m^3]	β_2 [N/m^5]	Residual norm
SREB	$1.1 \cdot 10^6$	$9.5 \cdot 10^4$	371.59	29.88	$0.075 \cdot 10^{-8}$	$2.2 \cdot 10^{-2}$
FREB	$4.6 \cdot 10^6$	$3.9 \cdot 10^5$	174.60	−506.64	1.48	$6.8 \cdot 10^{-2}$
PW16010L	$1.7 \cdot 10^6$	$2.7 \cdot 10^5$	593.0	0.076	$4.8 \cdot 10^{-5}$	$2.3 \cdot 10^{-3}$
PW16010T	$1.97 \cdot 10^6$	$2.8 \cdot 10^5$	832.9	0.81	0.001	$6.7 \cdot 10^{-3}$

Table 3
Averages of the identified constitutive parameters relevant to the experimental hysteresis loops. Refined optimization.

Test	k_a [N/m]	k_b [N/m]	α	β_1 [N/m^3]	β_2 [N/m^5]	Residual norm
SREB	$1.2 \cdot 10^6$	$8.0 \cdot 10^4$	504.44	$8.5 \cdot 10^5$	$5.4 \cdot 10^8$	$4.6 \cdot 10^{-3}$
FREB	$5.3 \cdot 10^6$	$3.7 \cdot 10^5$	280.43	$-2.4 \cdot 10^7$	$9.8 \cdot 10^8$	$7.6 \cdot 10^{-3}$
PW16010L	$1.8 \cdot 10^6$	$2.6 \cdot 10^5$	704.96	$1.0 \cdot 10^8$	$5.0 \cdot 10^{11}$	$8.2 \cdot 10^{-4}$
PW16010T	$2.1 \cdot 10^6$	$2.5 \cdot 10^5$	981.3	$1.04 \cdot 10^9$	$1.07 \cdot 10^{13}$	$1.7 \cdot 10^{-3}$

Please cite this article as: S. Sessa, N. Vaiana, M. Paradiso et al., An inverse identification strategy for the mechanical parameters of a phenomenological hysteretic constitutive model, Mechanical Systems and Signal Processing, https://doi.org/10.1016/j.ymssp.2020.106622

negligible imaginary part of the residual increases the value of the objective function. For this reason, it is convenient to perform a numerical check after the optimization procedure in order to avoid such a drawback.

Concerning the analyzed cases, all the identified parameters provide non-complex values of the response.

5. Conclusions

An inverse strategy for the identification of constitutive parameters characterizing materials modeled by the phenomenological model [42] has been developed. It is based on two optimization algorithms performed in sequence aiming to minimize a residual defined as the normalized mean-square error between a target experimental load-displacement curve and the response of the theoretical model proposed in [42].

To ensure robustness of the minimization procedures, a strategy for determining suitable first trials has been introduced in the algorithm. Specifically, trial parameters are computed by closed-form relationships analyzing physical properties of the experimental data, such as stiffness in peculiar regions of the experimental loops.

The procedure has been developed for the Algebraic Model presented in [42], currently the most versatile and comprehensive material developed within the phenomenological class [41]; however, it can be easily extended to other constitutive models belonging to the same family as detailed in the paper.

Effectiveness and efficiency of the proposed algorithm have been proved by a set of numerical applications. Specifically, the strategy has been applied to two artificial responses proving its theoretical soundness. Moreover, four experimental responses have been identified in order to investigate the performances of the proposed strategy for real case identifications.

The numerical results have proved the accuracy of the algorithm in determining constitutive parameters of the Algebraic Model since the load-displacement curves computed by the identified parameters correspond to very small residual norms and catch the main features, such as hardening at the loop edges, stiffness trend and inflection points, of all experimental tests.

The algebraic material developed in [42] has been also implemented in OpenSees [45], an open-source framework for finite-element analysis, in order to ensure replicability of the results and foster the dissemination of such a phenomenological model.

Uncited references

[8–10].

CRediT authorship contribution statement

Salvatore Sessa: Conceptualization, Methodology, Software, Writing - review & editing. **Nicoló Vaiana:** Validation, Data curation, Resources. **Massimo Paradiso:** Validation. **Luciano Rosati:** Supervision, Writing - review & editing, Funding acquisition.

Declaration of Competing Interest

The authors declare that they have no known competing financial interests or personal relationships that could have appeared to influence the work reported in this paper.

Funding and acknowledgments

This work was supported by the Italian Government, ReLuis 2017 project [AQ DPC/ReLUIS 2014-2018, PR2, Task 2.3] and PRIN 2015 grants [2015JW9NJT-PE8, WP2 Task 2.1], which are gratefully acknowledged by the authors.

Appendix A. OpenSees implementation of the Exponential and Algebraic Hysteretic Models

The Algebraic Material presented in [42] and described in Section 2.1 has been implemented in OpenSees v. 3.0, an open source, object-oriented framework for finite element analysis [45].

A beta version of such framework with the implemented material can be freely downloaded at the link [56] in which some sample application files are also provided.

The model belongs to the subclass *uniaxialMaterial* and its command line is:

```
uniaxialMaterial HystereticPoly $matTag $ka $kb $a $b1 $b2 $tol
```

in which `$matTag` is the progressive tag of the uniaxial material object, `$ka`-`$beta2` are the values of parameters $k_a, k_b, \alpha, \beta_1$ and β_2 and `$tol` is the value of the tolerance δ.

The implemented object contains methods implemented to address sensitivity analysis and supports the standard recorders to print strain, stress and stiffness (namely, `strain`, `stress`, `stressStrain` and `tangent`).

Please cite this article as: S. Sessa, N. Vaiana, M. Paradiso et al., An inverse identification strategy for the mechanical parameters of a phenomenological hysteretic constitutive model, Mechanical Systems and Signal Processing, https://doi.org/10.1016/j.ymssp.2020.106622

Appendix B. Report of the numerical applications

The present appendix reports in detail the numerical parameters and the outcomes of the identification procedures presented in Section 4. In particular, Tables B.4–B.7 report the initial trials and the outcomes of the preliminary optimization of the four considered experimental materials while Tables B.8–B.15 summarize the initial trials and the outcomes of the refined optimizations. Each one of these tables refers to a single branch of the considered hysteresis loops.

Table B.4
First trial values of the preliminary and refined optimizations. Test SREB. Tip cut $\delta_c = 10^{-4}$ m.

Branch	k_a^0 [N/m]	k_b^0 [N/m]	α^0	$\bar{k}_a^0$ [N/m]	$\bar{k}_b^0$ [N/m]	$\bar{\alpha}^0$	$\bar{\beta}_1^0$ [N/m^3]	$\bar{\beta}_2^0$ [N/m^5]
1	1.1e+06	8.0e+04	2.781e+02	1.1e+06	9.9e+04	3.864e+02	−3.51e+06	4.61e+09
2	9.7e+05	8.6e+04	2.776e+02	9.7e+05	9.8e+04	2.641e+02	−4.35e+06	5.08e+09
3	1.3e+06	8.7e+04	2.804e+02	1.3e+06	1.0e+05	4.859e+02	−1.78e+06	4.52e+09
4	1.1e+06	8.4e+04	2.781e+02	1.1e+06	8.4e+04	3.499e+02	2.39e+06	3.61e+09

Table B.5
First trial values of the preliminary and refined optimizations. Test FREB. Tip cut $\delta_c = 10^{-3}$ m.

Branch	k_a^0 [N/m]	k_b^0 [N/m]	α^0	$\bar{k}_a^0$ [N/m]	$\bar{k}_b^0$ [N/m]	$\bar{\alpha}^0$	$\bar{\beta}_1^0$ [N/m^3]	$\bar{\beta}_2^0$ [N/m^5]
1	1.4e+06	3.9e+05	1.315e+02	1.4e+06	3.9e+05	5.685e+01	−1.34e+07	3.75e+08
2	1.1e+07	5.3e+05	1.394e+02	1.1e+07	5.3e+05	3.772e+02	−2.61e+07	6.98e+08
3	1.4e+06	4.2e+05	1.297e+02	1.4e+06	2.5e+05	8.977e+01	−1.11e+07	3.48e+08

Table B.6
First trial values of the preliminary and refined optimizations. Test PW16010L. Tip cut $\delta_c = 2 \cdot 10^{-4}$ m.

Branch	k_a^0 [N/m]	k_b^0 [N/m]	α^0	$\bar{k}_a^0$ [N/m]	$\bar{k}_b^0$ [N/m]	$\bar{\alpha}^0$	$\bar{\beta}_1^0$ [N/m^3]	$\bar{\beta}_2^0$ [N/m^5]
1	1.8e+06	2.7e+05	1.750e+03	1.8e+06	2.6e+05	4.691e+02	4.22e+08	−3.54e+12
2	1.5e+06	3.1e+05	1.738e+03	1.5e+06	3.1e+05	7.068e+02	1.52e+08	4.28e+12
3	1.8e+06	2.2e+05	1.758e+03	1.8e+06	2.4e+05	4.222e+02	9.12e+07	3.11e+12
4	1.6e+06	3.3e+05	1.753e+03	1.6e+06	3.3e+05	7.195e+02	−8.55e+08	1.16e+13
5	1.8e+06	2.5e+05	1.759e+03	1.8e+06	2.4e+05	4.303e+02	2.46e+08	1.49e+12
6	1.6e+06	3.5e+05	1.743e+03	1.6e+06	3.5e+05	8.992e+02	2.44e+08	2.19e+12
7	1.8e+06	2.4e+05	1.750e+03	1.8e+06	2.4e+05	4.749e+02	3.10e+08	4.69e+11
8	1.6e+06	3.0e+05	1.745e+03	1.6e+06	3.1e+05	6.843e+02	−4.63e+08	1.02e+13
9	1.9e+06	2.3e+05	1.769e+03	1.9e+06	2.3e+05	5.306e+02	5.13e+08	1.19e+12

Table B.7
First trial values of the preliminary and refined optimizations. Test PW16010T. Tip cut $\delta_c = 2 \cdot 10^{-4}$ m.

Branch	k_a^0 [N/m]	k_b^0 [N/m]	α^0	$\bar{k}_a^0$ [N/m]	$\bar{k}_b^0$ [N/m]	$\bar{\alpha}^0$	$\bar{\beta}_1^0$ [N/m^3]	$\bar{\beta}_2^0$ [N/m^5]
1	1.8e+06	2.5e+05	1.752e+03	1.8e+06	3.0e+05	8.065e+02	2.63e+09	−1.24e+13
2	2.0e+06	2.1e+05	1.769e+03	2.0e+06	2.7e+05	5.192e+02	9.09e+08	1.27e+12
3	1.9e+06	2.9e+05	1.765e+03	1.9e+06	2.9e+05	1.093e+03	1.85e+09	−3.30e+12
4	2.2e+06	2.4e+05	1.767e+03	2.2e+06	2.6e+05	5.964e+02	1.77e+09	−7.27e+12
5	1.8e+06	2.8e+05	1.739e+03	1.8e+06	2.8e+05	1.078e+03	3.40e+09	−1.74e+13
6	2.1e+06	3.3e+05	1.753e+03	2.1e+06	3.3e+05	6.673e+02	6.25e+08	9.01e+11
7	1.9e+06	2.6e+05	1.768e+03	1.9e+06	2.6e+05	9.791e+02	2.26e+09	−2.12e+12
8	2.2e+06	2.6e+05	1.781e+03	2.2e+06	2.9e+05	6.714e+02	9.99e+08	−2.24e+11
9	1.9e+06	2.7e+05	1.760e+03	1.9e+06	2.7e+05	1.085e+03	2.95e+09	−1.20e+13

Table B.8
Identified constitutive parameters relevant to test SREB. Preliminary optimization.

Branch	k_a [N/m]	k_b [N/m]	α	β_1 [N/m^3]	β_2 [N/m^5]	Residual norm
1	1.1e+06	9.9e+04	3.864e+02	4.69e+01	1.39e−01	2.2e−02
2	9.7e+05	9.8e+04	2.641e+02	3.19e+01	1.02e−01	1.8e−02
3	1.3e+06	1.0e+05	4.859e+02	4.06e+01	5.84e−02	2.2e−02
4	1.1e+06	8.4e+04	3.499e+02	5.20e−05	7.10e−08	2.4e−02

Please cite this article as: S. Sessa, N. Vaiana, M. Paradiso et al., An inverse identification strategy for the mechanical parameters of a phenomenological hysteretic constitutive model, Mechanical Systems and Signal Processing, https://doi.org/10.1016/j.ymssp.2020.106622

Table B.9
Identified constitutive parameters relevant to test FREB. Preliminary optimization.

Branch	k_a [N/m]	k_b [N/m]	α	β_1 [N/m^3]	β_2 [N/m^5]	Residual norm
1	1.4e+06	3.9e+05	5.685e+01	−5.33e−05	−2.67e−07	6.0e−02
2	1.1e+07	5.3e+05	3.772e+02	1.59e−05	2.96e−09	1.2e−01
3	1.4e+06	2.5e+05	8.977e+01	−1.52e+03	4.45e+00	2.6e−02

Table B.10
Identified constitutive parameters relevant to test PW16010L. Preliminary optimization.

Branch	k_a [N/m]	k_b [N/m]	α	β_1 [N/m^3]	β_2 [N/m^5]	Residual norm
1	1.8e+06	2.6e+05	4.691e+02	−2.64e−01	−8.42e−12	5.5e−04
2	1.5e+06	3.1e+05	7.068e+02	−7.83e−05	0.00e+00	2.7e−03
3	1.8e+06	2.4e+05	4.222e+02	7.68e−01	4.59e−04	1.7e−03
4	1.6e+06	3.3e+05	7.195e+02	−2.95e−05	0.00e+00	1.3e−03
5	1.8e+06	2.4e+05	4.303e+02	−3.77e−01	−2.84e−05	1.2e−03
6	1.6e+06	3.5e+05	8.992e+02	−6.61e−05	6.86e−14	4.2e−03
7	1.8e+06	2.4e+05	4.749e+02	−7.54e−04	0.00e+00	1.6e−03
8	1.6e+06	3.1e+05	6.843e+02	5.56e−01	7.29e−06	2.7e−03
9	1.9e+06	2.3e+05	5.306e+02	−7.54e−04	0.00e+00	4.3e−03

Table B.11
Identified constitutive parameters relevant to test PW16010T. Preliminary optimization.

Branch	k_a [N/m]	k_b [N/m]	α	β_1 [N/m^3]	β_2 [N/m^5]	Residual norm
1	1.8e+06	3.0e+05	8.065e+02	2.05e+00	1.81e−04	6.4e−03
2	2.0e+06	2.7e+05	5.192e+02	2.53e+00	1.17e−02	4.0e−03
3	1.9e+06	2.9e+05	1.093e+03	−4.72e−05	0.00e+00	7.6e−03
4	2.2e+06	2.6e+05	5.964e+02	1.22e+00	0.00e+00	5.0e−03
5	1.8e+06	2.8e+05	1.078e+03	−1.66e−05	0.00e+00	8.0e−03
6	2.1e+06	3.3e+05	6.673e+02	−4.04e−04	0.00e+00	7.9e−03
7	1.9e+06	2.6e+05	9.791e+02	−1.27e−04	0.00e+00	8.7e−03
8	2.2e+06	2.9e+05	6.714e+02	1.46e+00	3.35e−14	3.9e−03
9	1.9e+06	2.7e+05	1.085e+03	−2.36e−05	1.43e−13	9.2e−03

Table B.12
Identified constitutive parameters relevant to test SREB. Refined optimization.

Branch	k_a [N/m]	k_b [N/m]	α	β_1 [N/m^3]	β_2 [N/m^5]	Residual norm
1	1.5e+06	7.9e+04	6.907e+02	2.60e+06	5.28e+09	4.8e−03
2	1.4e+06	8.3e+04	4.883e+02	−2.94e+06	6.28e+09	5.2e−03
3	1.0e+06	7.8e+04	4.896e+02	4.73e+06	4.50e+09	3.7e−03
4	1.0e+06	8.2e+04	3.492e+02	−9.72e+05	5.57e+09	4.8e−03

Table B.13
Identified constitutive parameters relevant to test FREB. Refined optimization.

Branch	k_a [N/m]	k_b [N/m]	α	β_1 [N/m^3]	β_2 [N/m^5]	Residual norm
1	8.4e+06	3.7e+05	4.693e+02	−2.70e+07	1.15e+09	9.1e−03
2	6.0e+06	3.8e+05	3.004e+02	−2.32e+07	9.02e+08	7.1e−03
3	1.6e+06	3.6e+05	7.160e+01	−2.31e+07	8.90e+08	6.5e−03

Table B.14
Identified constitutive parameters relevant to test PW16010L. Refined optimization.

Branch	k_a [N/m]	k_b [N/m]	α	β_1 [N/m^3]	β_2 [N/m^5]	Residual norm
1	1.9e+06	2.6e+05	4.989e+02	2.90e+08	−2.60e+12	4.4e−04
2	1.8e+06	3.1e+05	8.733e+02	−2.28e+08	1.08e+13	1.0e−03
3	1.4e+06	1.9e+05	3.186e+02	1.53e+08	5.39e+12	7.5e−04
4	1.5e+06	3.3e+05	6.517e+02	−8.16e+08	1.19e+13	4.2e−04
5	1.5e+06	2.1e+05	3.561e+02	−1.51e+08	8.36e+12	3.2e−04
6	2.8e+06	3.4e+05	1.871e+03	−3.17e+08	8.58e+12	2.5e−03
7	1.8e+06	2.2e+05	4.789e+02	9.17e+08	−3.34e+12	3.6e−04
8	1.8e+06	3.0e+05	8.537e+02	2.75e+08	6.15e+12	1.2e−03
9	1.7e+06	2.2e+05	4.429e+02	8.00e+08	−4.34e+11	2.8e−04

Please cite this article as: S. Sessa, N. Vaiana, M. Paradiso et al., An inverse identification strategy for the mechanical parameters of a phenomenological hysteretic constitutive model, Mechanical Systems and Signal Processing, https://doi.org/10.1016/j.ymssp.2020.106622

Table B.15
Identified constitutive parameters relevant to test PW16010T. Refined optimization.

Branch	k_a [N/m]	k_b [N/m]	α	β_1 [N/m^3]	β_2 [N/m^5]	Residual norm
1	2.0e+06	2.5e+05	1.062e+03	1.55e+09	8.74e+12	1.9e−03
2	2.1e+06	2.0e+05	6.178e+02	3.18e+09	−1.81e+13	4.9e−04
3	1.8e+06	2.8e+05	1.075e+03	5.24e+08	1.81e+13	2.2e−03
4	2.2e+06	2.1e+05	6.949e+02	1.80e+09	1.32e+12	1.9e−03
5	2.6e+06	2.8e+05	1.639e+03	1.54e+08	2.36e+13	2.5e−03
6	2.3e+06	3.1e+05	8.810e+02	−1.31e+09	3.23e+13	3.0e−03
7	1.8e+06	2.6e+05	9.314e+02	8.24e+08	1.81e+13	1.4e−03
8	2.2e+06	2.5e+05	7.445e+02	1.58e+09	−3.89e+10	1.0e−03
9	2.1e+06	2.7e+05	1.186e+03	1.06e+09	1.19e+13	1.3e−03

Appendix C. Supplementary data

Supplementary data associated with this article can be found, in the online version, at https://doi.org/10.1016/j.ymssp.2020.106622.

References

[1] M. Dimian, P. Andrei, Phenomena in Hysteretic Systems, first ed., Springer, New York, NY, USA, 2008.
[2] X.-X. Bai, F.-L. Cai, P. Chen, Resistor-capacitor (RC) operator-based hysteresis model for magnetorheological (MR) dampers, Mech. Syst. Signal Process. 117 (2019) 157–169.
[3] A. Visintin, On hysteresis in elasto-plasticity and in ferromagnetism, Int. J. Non-Linear Mech. 37 (8) (2002) 1283–1298.
[4] H. Wittke, J. Olfe, K.-T. Rie, Description of stress-strain hysteresis loops with a simple approach, Int. J. Fatigue 19 (2) (1997) 141–149.
[5] I. Nuzzo, D. Losanno, N. Caterino, G. Serino, L.M.B. Rotondo, Experimental and analytical characterization of steel shear links for seismic energy dissipation, Eng. Struct. 172 (2018) 405–418.
[6] B. Bahn, C.-T. Hsu, Stress-strain behavior of concrete under cyclic loading, ACI Mater. J. 95 (2) (1998) 178–193.
[7] J. Hwang, J. Wu, T.-C. Pan, G. Yang, A mathematical hysteretic model for elastomeric isolation bearings, Earthq. Eng. Struct. Dyn. 31 (4) (2002) 771–789.
[8] M. Kikuchi, I. Aiken, An analytical hysteresis model for elastomeric seismic isolation bearings, Earthq. Eng. Struct. Dyn. 26 (2) (1997) 215–231.
[9] D. Losanno, I.E.M. Sierra, M. Spizzuoco, J. Marulanda, P. Thomson, Experimental assessment and analytical modeling of novel fiber-reinforced isolators in unbounded configuration, Compos. Struct. 212 (2019) 66–82.
[10] I.E.M. Sierra, D. Losanno, S. Strano, J. Marulanda, P. Thomson, Development and experimental behavior of HDR seismic isolators for low-rise residential buildings, Eng. Struct. 183 (2019) 894–906.
[11] I. Nuzzo, D. Losanno, N. Caterino, Seismic design and retrofit of frame structures with hysteretic dampers: a simplified displacement-based procedure, Bull. Earthq. Eng. 17 (5) (2019) 2787–2819.
[12] G. Puel, B. Bourgeteau, D. Aubry, Parameter identification of nonlinear time-dependent rubber bushings models towards their integration in multibody simulations of a vehicle chassis, Mech. Syst. Signal Process. 36 (2) (2013) 354–369.
[13] D. Badoni, N. Makris, Nonlinear response of single piles under lateral inertial and seismic loads, Soil Dyn. Earthq. Eng. 15 (1) (1996) 29–43.
[14] J. Song, A. Der Kiureghian, J. Sackman, Seismic interaction in electrical substation equipment connected by non-linear rigid bus conductors, Earthq. Eng. Struct. Dyn. 36 (2) (2007) 167–190.
[15] T. Baber, M. Noori, Random vibration of degrading, pinching systems, J. Eng. Mech. 111 (8) (1985) 1010–1026.
[16] Y.-K. Wen, Method for random vibration of hysteretic systems, ASCE J. Eng. Mech. Div. 102 (2) (1976) 249–263.
[17] J. Noel, G. Kerschen, Nonlinear system identification in structural dynamics: 10 more years of progress, Mech. Syst. Signal Process. 83 (2017) 2–35.
[18] B. Carboni, W. Lacarbonara, P. Brewick, S. Masri, Dynamical response identification of a class of nonlinear hysteretic systems, J. Intell. Mater. Syst. Struct. 29 (13) (2018) 2795–2810.
[19] G. Formica, M. Taló, G. Lanzara, W. Lacarbonara, Parametric identification of carbon nanotube nanocomposites constitutive response, J. Appl. Mech. Trans. ASME 86 (4) (2019).
[20] R. Bouc, Modele mathematique d'hysteresis, Acustica 24 (1971) 16–25.
[21] Y. Wen, Equivalent linearization for hysteretic systems under random excitation, J. Appl. Mech. Trans. ASME 47 (1) (1980) 150–154.
[22] M. Hodgdon, Mathematical theory and calculations of magnetic hysteresis curves, IEEE Trans. Magn. 24 (6) (1988) 3120–3122.
[23] D. Jiles, D. Atherton, Theory of ferromagnetic hysteresis (invited), J. Appl. Phys. 55 (6) (1984) 2115–2120.
[24] J. Song, A. Der Kiureghian, Generalized Bouc-Wen model for highly asymmetric hysteresis, J. Eng. Mech. 132 (6) (2006) 610–618.
[25] M. Ismail, F. Ikhouane, J. Rodellar, The hysteresis Bouc-Wen model, a survey, Arch. Comput. Methods Eng. 16 (2) (2009) 161–188.
[26] V. Hassani, T. Tjahjowidodo, T.N. Do, A survey on hysteresis modeling, identification and control, Mech. Syst. Signal Process. 49 (1) (2014) 209–233.
[27] K. Worden, G. Manson, On the identification of hysteretic systems. Part I: fitness landscapes and evolutionary identification, Mech. Syst. Signal Process. 29 (2012) 201–212.
[28] K. Worden, W. Becker, On the identification of hysteretic systems. Part II: Bayesian sensitivity analysis and parameter confidence, Mech. Syst. Signal Process. 29 (2012) 213–227.
[29] K. Worden, J. Hensman, Parameter estimation and model selection for a class of hysteretic systems using Bayesian inference, Mech. Syst. Signal Process. 32 (2012) 153–169.
[30] Y. Lei, D. Xia, K. Erazo, S. Nagarajaiah, A novel unscented Kalman filter for recursive state-input-system identification of nonlinear systems, Mech. Syst. Signal Process. 127 (2019) 120–135.
[31] A. Charalampakis, C. Dimou, Identification of Bouc-Wen hysteretic systems using particle swarm optimization, Comput. Struct. 88 (21–22) (2010) 1197–1205.
[32] G. Dimopoulos, Mixed-variable engineering optimization based on evolutionary and social metaphors, Comput. Methods Appl. Mech. Eng. 196 (4–6) (2007) 803–817.
[33] A.F. Esfahani, P. Dreesen, K. Tiels, J.-P. Nol, J. Schoukens, Parameter reduction in nonlinear state-space identification of hysteresis, Mech. Syst. Signal Process. 104 (2018) 884–895.
[34] J. Noel, A. Esfahani, G. Kerschen, J. Schoukens, A nonlinear state-space approach to hysteresis identification, Mech. Syst. Signal Process. 84 (2017) 171–184.
[35] C. Dimou, V. Koumousis, Reliability-based optimal design of truss structures using particle swarm optimization, J. Comput. Civil Eng. 23 (2) (2009) 100–109.

Please cite this article as: S. Sessa, N. Vaiana, M. Paradiso et al., An inverse identification strategy for the mechanical parameters of a phenomenological hysteretic constitutive model, Mechanical Systems and Signal Processing, https://doi.org/10.1016/j.ymssp.2020.106622

[36] S. Gholizadeh, E. Salajegheh, Optimal design of structures subjected to time history loading by swarm intelligence and an advanced metamodel, Comput. Methods Appl. Mech. Eng. 198 (37–40) (2009) 2936–2949.
[37] W. Ramberg, W. Osgood, Description of stress-strain curves by three parameters (Tech. rep.), National Advisory Committee on Aeronautics, 1943.
[38] M. Menegotto, P. Pinto, Method of analysis for cyclically loaded r.c. plane frames including changes in geometry and non-elastic behavior of elements under combined normal force and bending, in: Proceedings of IABSE Symposium on Resistance and Ultimate Deformability of Structures Acted on by Well-Defined Repeated Loads, 1973, Lisbon, Portugal.
[39] H. Hauser, Energetic model of ferromagnetic hysteresis, J. Appl. Phys. 75 (5) (1994) 2584–2597.
[40] A. Pacitti, M. Peigney, F. Bourquin, W. Lacarbonara, Experimental data based cable tension identification via nonlinear static inverse problem, Proc. Eng. 199 (2017) 453–458.
[41] N. Vaiana, S. Sessa, F. Marmo, L. Rosati, A class of uniaxial phenomenological models for simulating hysteretic phenomena in rate-independent mechanical systems and materials, Nonlinear Dyn. 93 (3) (2018) 1647–1669.
[42] N. Vaiana, S. Sessa, F. Marmo, L. Rosati, An accurate and computationally efficient uniaxial phenomenological model for steel and fiber reinforced elastomeric bearings, Compos. Struct. 211 (2019) 196–212.
[43] N. Vaiana, S. Sessa, F. Marmo, L. Rosati, Nonlinear dynamic analysis of hysteretic mechanical systems by combining a novel rate-independent model and an explicit time integration method, Nonlinear Dyn.https://doi.org/10.1007/s11071-019-05022-5..
[44] L. Liu, W. Liu, D. Cartes, Particle swarm optimization-based parameter identification applied to permanent magnet synchronous motors, Eng. Appl. Artif. Intell. 21 (7) (2008) 1092–1100.
[45] S. Mazzoni, F. McKenna, M.H. Scott, G.L. Fenves, et al., Opensees command language manual, Pacific Earthquake Engineering Research (PEER) Center..
[46] A. Tarantola, Inverse problem theory: methods for data fitting and model parameter estimation, 1987. .
[47] R. Fedele, S. Sessa, N. Valoroso, Image correlation-based identification of fracture parameters for structural adhesives, Tech. Mech. 32 (2) (2012) 195–204.
[48] N. Valoroso, S. Sessa, M. Lepore, G. Cricrí, Identification of mode-I cohesive parameters for bonded interfaces based on DCB test, Eng. Fract. Mech. 104 (2013) 56–79.
[49] R. Byrd, M. Hribar, J. Nocedal, An interior point algorithm for large-scale nonlinear programming, SIAM J. Optim. 9 (4) (1999) 877–900.
[50] C.S. Tsai, T.-C. Chiang, B.-J. Chen, S.-B. Lin, An advanced analytical model for high damping rubber bearings, Earthq. Eng. Struct. Dyn. 32 (9) (2003) 1373–1387.
[51] J. Kelly, S. Takhirov, Analytical and experimental study of fiber-reinforced elastomeric isolators (Tech. rep.), PEER Report 2001/11, Pacific Earthquake Engineering Research Center, University of California, Berkeley, CA, USA, 2001.
[52] N. Vaiana, M. Spizzuoco, G. Serino, Wire rope isolators for seismically base-isolated lightweight structures: experimental characterization and mathematical modeling, Eng. Struct. 140 (2017) 498–514.
[53] S. Sessa, External repository of load-displacement experimental responses, last visited: December 2019 (2019). URL:http://bit.ly/2PlcCCZ..
[54] T. Coleman, Y. Li, An interior trust region approach for nonlinear minimization subject to bounds, SIAM J. Optim. 6 (2) (1996) 418–445.
[55] R. Waltz, J. Morales, J. Nocedal, D. Orban, An interior algorithm for nonlinear optimization that combines line search and trust region steps, Math. Program. 107 (3) (2006) 391–408.
[56] S. Sessa, Modified OpenSees vol 3.0.3 executable, last visited: December 2019 (2019). URL:http://bit.ly/2OTHiLE..

Please cite this article as: S. Sessa, N. Vaiana, M. Paradiso et al., An inverse identification strategy for the mechanical parameters of a phenomenological hysteretic constitutive model, Mechanical Systems and Signal Processing, https://doi.org/10.1016/j.ymssp.2020.106622